Hindawi
International Journal of Photoenergy
Volume 2023, Article ID 9931481, 17 pages
https://doi.org/10.1155/2023/9931481

Research Article

A New Hybrid MPPT Based on Incremental Conductance-Integral Backstepping Controller Applied to a PV System under Fast-Changing Operating Conditions

Ambe Harrison,[1] **Njimboh Henry Alombah**,[2] **and Jean de Dieu Nguimfack Ndongmo**[3]

[1]*Department of Electrical and Electronics Engineering, College of Technology (COT), University of Buea, P.O. Box Buea 63, Cameroon*
[2]*Department of Electrical and Electronics Engineering, College of Technology, University of Bamenda, P.O. Box 39, Bambili, Cameroon*
[3]*Department of Electrical and Power Engineering, Higher Technical Teacher Training College (HTTTC), University of Bamenda, P.O. Box 39 Bambili, Cameroon*

Correspondence should be addressed to Njimboh Henry Alombah; henry.alombah@gmail.com

Received 22 November 2022; Revised 28 January 2023; Accepted 3 February 2023; Published 15 February 2023

Academic Editor: Alberto Álvarez-Gallegos

Maximum power point tracking (MPPT) is becoming more and more important in the optimization of photovoltaic systems. Several MPPT algorithms and nonlinear controllers have been developed for improving the energy yield of PV systems. On the one hand, most of the conventional algorithms such as the incremental conductance (INC) demonstrate a good affinity for the maximum power point (MPP) but often fail to ensure acceptable stability and robustness of the PV system against fast-changing operating conditions. On the other hand, the MPPT nonlinear controllers can palliate the robust limitations of the algorithms. However, most of these controllers rely on expensive solar irradiance measurement systems or complex and relatively less accurate methods to seek the maximum power voltage. In this paper, we propose a new hybrid MPPT based on the incremental conductance algorithm and the integral backstepping controller. The hybrid scheme exploits the benefits of the INC algorithm in seeking the maximum power voltage and feeds a nonlinear integral backstepping controller whose stability was ensured by the Lyapunov theory. Therefore, in terms of characteristics, the overall system is a blend of the MPP-seeking potential of the INC and the nonlinear and robust potentials of the integral backstepping controller (IBSC). It was noted that the hybrid system successfully palliates the conventional limitations of the isolated INC and relieves the PV system from the expensive burden of solar irradiance measurement. The proposed hybrid system increased the operational efficiency of the PV system to 99.94% and was found better than the INC MPPT algorithm and 8 other recently published MPPT methods. An extended validation under experimental environmental conditions showed that the hybrid system is approximately four times faster than the INC in tracking the maximum power with better energy yield than the latter.

1. Introduction

The energy sector has a significant influence on our climate and environment as it contributes to roughly two-thirds of all harmful greenhouse gas emissions [1]. There is a need for these emissions to be reduced significantly, which can only be achieved by phasing out fossil fuels. Therefore, a sustainable revision of the energy sector should be an important consideration in relieving the world of the problems of climate change and global warming. The 2015 Paris Agreement on climate change mandates the transition to renewable energy generation to limit the rise of global temperatures to well below 2 degrees Celsius and ideally below 1.5 degrees Celsius above preindustrial levels [2]. During the recent decade, several renewable energy sources have been sought, amongst which solar energy is one of the most

reliable and sustainable. The prominent nature of solar energy is attributable to its environmental friendliness and global abundance [3–7]. Consequently, global solar photovoltaic (PV) generation has been on the rise, with a recent increase from 823.8 terawatt-hours (TWH) to 1002.9 TWh [8]. However, according to the International Energy Agency (IEA), an annual global PV generation of approximately 7400 TWh by 2030, aligning with the net zero greenhouse gas scenario, from the current 1002.9 TWh requires annual average generation growth of about 25% during 2020-2030. Despite the high drift towards solar PV systems, there are two main challenges to their exploitation: low efficiency and high financial cost of installation. To avoid ambiguity with the term efficiency, it is worthy to distinguish the two types of efficiency related to the PV: conversion efficiency which is related to the technology of the solar cells and operational efficiency which is related to the electrical operation of the PV system. This work focuses on operational efficiency. There are two ways to improve the cost and compensate for the operational efficiency of PV systems: on the one hand, the structure of the PV generator is changed at the implementation stage or the PV system is forced to operate at its maximum energy potential [9]. The latter approach is the maximum power point tracking algorithm and focus of this paper.

In the recent decade, numerous maximum power point tracking algorithms have been deployed in the literature [10–22]. These algorithms differ in cost, complexity, and performance. A retrospective survey shows that perturb and observe is one of the most popular algorithms for MPPT in PV systems. However, this algorithm suffers from several limitations: oscillations under fast-changing operating conditions, loss of tracking direction under fast-changing irradiance, and the trade-off between dynamic response and steady-state oscillations. Given the ease of implementation and simplicity of this algorithm, numerous efforts are being vested to alleviate its aforementioned problem. The incremental conductance (INC), which is an improved variant of perturb and observe (P&O), can perceive that the maximum power point (MPP) has been attained, hence overcoming the disadvantages of P&O [23]. Even though the INC provides better accuracy than P&O under fast-changing irradiance conditions, it still cannot guarantee finite stability of the operating point around the neighborhood of the maximum power point. The adaptive variable step-size algorithm P&O in [24, 25] improves the decision in making the P&O perturbation step; however, it does not solve the problem of stabilization of the operating point at the MPP, especially under fast-changing operating conditions. The beta algorithm proposed in [26–28] addressed the trade-off problem in the conventional P&O; however, its complete dependency on the latter is a serious limitation of the method.

Numerous other schemes such as the intelligent and optimization algorithms including artificial neural networks [29], fuzzy logic [29–32], particle swarm optimization [33], ant colony optimization [34], and grey wolf optimizer [35, 36] have recently received attention with regard to MPPT. The optimization algorithms provide a better solution to the tracking performance of the conventional P&O and INC; however, the problem of the stability of the MPP is still recurrent. The ANN MPPT approach on the other hand is considered one of the most successful approaches for MPPT. This is because a trained intelligent model has better recognition capability of the MPP under any environmental conditions. However, the ANN method always fails to ensure satisfactory performance under varying load scenarios.

It is a fact that the maximum power point stability problem especially under fast-changing operating conditions presented by the above MPPT algorithms is due to their lack of nonlinear capacity. This is even obvious given that the PV generator is a nonlinear system, coupled to the nonlinear time-variant nature of power electronic converters used for their control. It is therefore a better choice to seek nonlinear techniques that can ensure the stability of the PV system under changing operating conditions and at the same time provide good efficiency in the tracking mechanism.

In the light of nonlinear control of the PV generator, some controllers have been proposed in the literature. The sliding mode controller (SMC) in [37–39] provides robust performance under changing operating conditions; however, the discontinuous nature of the SMC nonlinear control law introduces chattering problems [40], defined in [41] as "finite amplitude oscillations." The synergic controller (SC) which is an improved nonlinear control strategy that has recently been applied to the maximum power point control of the PV system [40, 42] presented better performance than the SMC. The prominence of the SC lies in the continuity of its control law, hence solving the chattering problem [42].

Another class of advanced nonlinear controllers superior to the SC is the backstepping controller (BSC), based on the recursive Lyapunov design that has been applied to the MPPT control of PV systems [43]. Though a comparison between SC and BSC in an MPPT context has not been well established, the work in [44] shows that in a class of nonlinear systems out of the MPPT context, the BSC outclassed the SC. Though exceptional in performance, however, unknown dynamics are usually not modeled in the BSC controller design; consequently, the controller usually presents steady-state errors. To allow good robustness of the controller against unmodeled dynamics and perturbations, an integral action was added to form the integral backstepping controller [45, 46].

From the presented literature survey and trend of nonlinear controllers, it can be seen that the backstepping and its integral improvement are the most prominent within the context of MPPT. However, as in every closed-loop control system topology, the controller has to be properly fed with an accurate reference. This is where the above-presented controllers show serious limitations. In all the above nonlinear techniques, the reference (maximum power voltage) is generated using either an offline-trained regression plane [45] or offline-trained neural network-based techniques [46]. The offline-trained network requires frequent maintenance once deployed in the field because it will be subject to wear and tear. However, the main limitation of these offline-trained models for reference generation is the

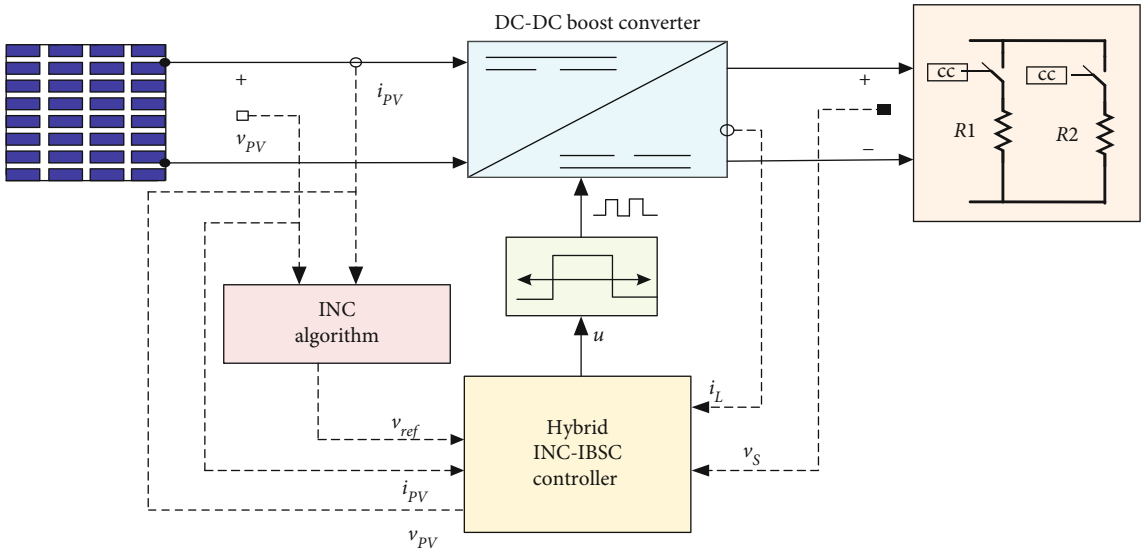

Figure 1: Synoptic diagram of the proposed hybrid MPPT system.

fact that when used in the PV system, it requires a very expensive solar irradiance sensor (pyranometer).

In this paper, we present a novel hybrid controller based on incremental conductance-integral backstepping (INC-IBSC). The hybrid MPPT controller exploits the benefit of the incremental conductance algorithm in seeking the maximum power point and the nonlinear stability and robustness of the integral backstepping controller. Firstly, the proposed system alleviates the problem of poor tracking performance under fast-changing operating conditions, exhibited by the conventional INC algorithm, and finally, it relieves the MPPT system from the cost burden of the irradiance sensor. In-depth numerical investigations proved the good robust performance of the controller under fast-changing operating conditions. The proposed hybrid system was found better than the conventional INC MPPT algorithm and eight other recently published methods in the literature.

The rest of this paper is organized as follows: in Section 2, a general description of the proposed system is presented. The incremental conductance algorithm is overviewed in Section-3. The mathematical modeling of the boost converter is described in Section 4 while the nonlinear controller is designed step by step in Section 5. Numerous investigations and numerical simulations are discussed in Section 6 while the paper is concluded in Section 7.

2. General Description of the Proposed System

The synoptic diagram of the proposed system is presented in Figure 1. It consists of an MSX-60 PV whose mathematical model is obtained according to [23], a DC-DC boost converter, a DC load, and the hybrid incremental conductance-integral backstepping controller (INC-IBSC).

The 60-watt PV is the main generator in the system that we desire to control. The incremental conductance algorithm, in its conventional form, generates a reference voltage that is fed into the INC-IBSC. The controller in its nonlinear capacity generates the nonlinear control law that modulates a pulse width signal which in turn drives the system via the boost converter coupled to the DC-variable load.

3. Incremental Conductance Algorithm (INC)

The incremental conductance (INC) algorithm is one of the most popular MPP algorithms [15, 47]. The method derives its name from the fact that the conductance of the PV is used to determine the movement towards the maximum power point (MPP). The basic principle of the algorithm is presented in Figure 2, while its mathematical description is as follows.

$$V_{\text{ref}} = \begin{cases} V + \delta V, & \dfrac{\Delta I_{\text{pv}}}{\Delta V_{\text{pv}}} > -\dfrac{I_{\text{pv}}}{V_{\text{pv}}}, \\ V + 0, & \dfrac{\Delta I_{\text{pv}}}{\Delta V_{\text{pv}}} = -\dfrac{I_{\text{pv}}}{V_{\text{pv}}}, \\ V - \delta V, & \dfrac{\Delta I_{\text{pv}}}{\Delta V_{\text{pv}}} < -\dfrac{I_{\text{pv}}}{V_{\text{pv}}}, \end{cases} \tag{1}$$

where ΔI_{pv}, ΔV_{pv}, and ΔV_{pv} are the change in current, voltage, and power due to voltage step size δV.

The operation of the INC is summarized in Equation (1) and Figure 2. It holds that when the operating point is to the left of the MPP, the reference voltage, V_{ref} is increased by a step δV to the MPP point. To the right of the MPP, the reference voltage is reduced by the same step. Continuous adjustment of the operating point according to Equation (1) moves the PV point at the MPP. To this end, the benefit of the INC as presented shall be exploited in a hybrid scheme by the nonlinear controller.

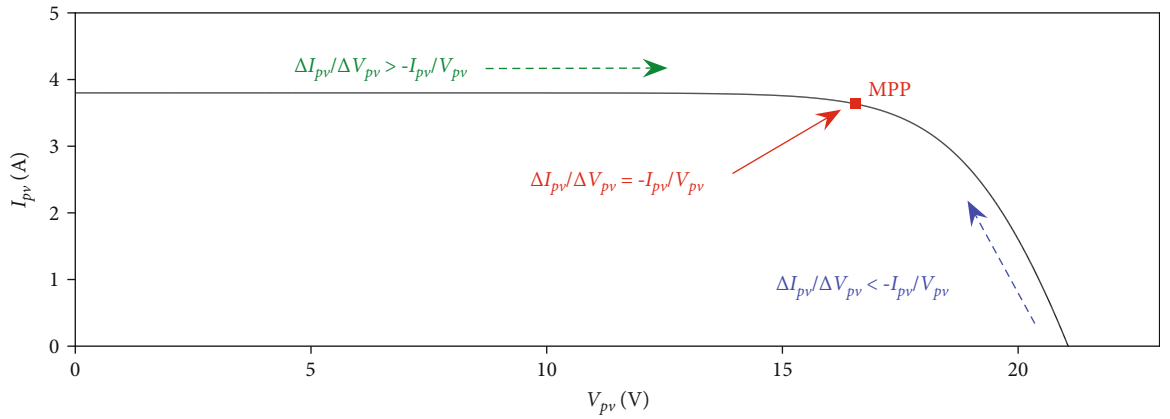

Figure 2: Graphical demonstration of the INC algorithm.

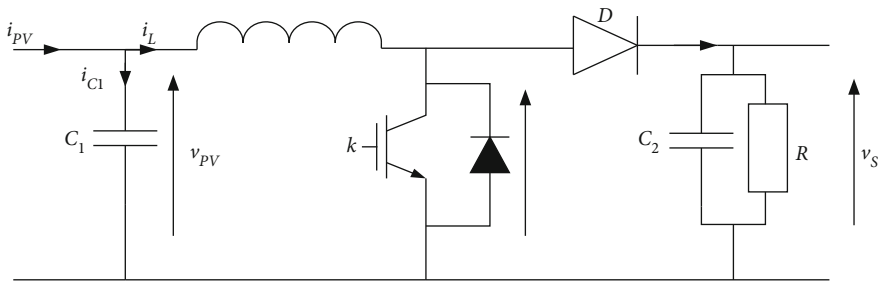

Figure 3: Electrical model of the DC-DC boost converter.

4. Mathematical Modeling of the Boost Converter

The boost converter is a switched-mode step-down DC-DC converter. A DC-DC converter is the key component of every MPPT system as it ensures impedance matching between the PV source and the load. The boost converter as shown in Figure 3 is made of an inductor (L) carrying current i_L, input capacitor (C_1) carrying current i_{c1} with the PV voltage V_{PV} at its terminals, a transistor switch (k), diode D, and output storage capacitor (C_2) in parallel with the load R. In this paper, the converter is considered to operate in continuous conduction mode (CCM). Furthermore, it is assumed that parasitic components in the inductor and capacitors are zero. In CCM, the converter operates in two modes. In mode 1, the switch k is on while the diode D is off. In the second mode of operation, the switch is off while diode D conducts.

The dynamic models for the two operating modes described above can be obtained using Kirchhoff's laws and are given in Equations (2) and (3) for mode 1 and mode 2, respectively [48]:

The state-space average model in Equation (4) is obtained from the dynamics of the two operating modes and is obtained as described in [48]:

$$\begin{cases} i_{c1} = i_{\mathrm{PV}} - i_L, \\ v_L = v_{\mathrm{PV}}, \\ i_{c2} = -\dfrac{v_S}{R}, \end{cases} \tag{2}$$

$$\begin{cases} i_{c1} = i_{\mathrm{PV}} - i_L, \\ v_L = v_{\mathrm{PV}} - v_S, \\ i_{c2} = i_L - \dfrac{v_S}{R}. \end{cases} \tag{3}$$

$$\begin{cases} \dot{x_1} = i_{\mathrm{PV}} - \dfrac{x_2}{C_1} \\ \dot{x_2} = \dfrac{x_1}{L} - \dfrac{x_3}{L}(1-u) \\ \dot{x_3} = \dfrac{x_2}{C_2}(1-u) - \dfrac{x_3}{C_2 R} \end{cases} \tag{4}$$

where $[x_1\, x_2\, x_3]^T = [\, v_{c1} \quad i_L \quad v_s \,]^T = x$ are the average state variables, with v_{c1}, i_L, and v_s denoting the input PV voltage, inductor current, and output voltage, respectively. The control law is denoted u.

Equation (4) which is the dynamical equation can then be exploited by a nonlinear controller

Assumption 1. All the state variables of the model are continuous and bounded.

Assumption 2. i_{PV}, x_1, x_2, and x_3 are accessible for measurement.

5. Nonlinear Control Design

The nonlinear controller is synthesized in this section. The controller receives a reference voltage from the INC

algorithm and exploits the dynamics of the converter to drive the PV system at the MPP. The controller proposed in this work is the integral backstepping controller (IBSC), whose design is based on Lyapunov theory. Let the voltage fed to the controller be V_{ref}.We recall that V_{ref}.is generated by the INC algorithm. Since this variable is the first state of the system, we can write that

$$x_{1\text{ref}} = V_{\text{ref}}. \tag{5}$$

Let e_1 be the first error considered in the Lyapunov design; we define it as the difference between the actual PV voltage and the reference from the INC algorithm, written mathematically as

$$e_1 = x_1 - x_{1\text{ref}}. \tag{6}$$

We have to label out the dynamics of this error, by taking its derivative written as

$$\dot{e}_1 = \dot{x}_1 - \dot{x}_{1\text{ref}} = \frac{i_{\text{PV}}}{C_1} - \frac{x_2}{C_1} - \dot{x}_{1\text{ref}}. \tag{7}$$

Introducing the integral action p to this error results in a macrovariable:

$$e = e_1 + p, \tag{8}$$

$$p = \int_o^t (e_1)dt = \int_o^t (x_1 - x_{1\text{ref}})dt. \tag{9}$$

It is worth noting that the integral action is introduced to allow good robustness of the controller against unmodeled dynamics and perturbations.

To ensure the stability of the controller, Lyapunov functions are introduced. Therefore, let V_1 be a positive definite Lyapunov function for ensuring stability, tracking, and convergence to the reference voltage from the INC algorithm. According to the Lyapunov theory, e_1 converges to zero if the first derivative of the Lyapunov function is negative definite. To this end, let the Lyapunov function be

$$V_1 = \frac{1}{2}e_1^2 + \frac{k}{2}p^2, \tag{10}$$

where $k > 0$.

Taking the first derivative of Equation (10) results to

$$\dot{V}_1 = e_1\dot{e}_1 + kp\dot{p}. \tag{11}$$

Inserting Equation (7) and the derivative of Equation (9) into (11) gives

$$\dot{V}_1 = e_1\left(\frac{i_{\text{PV}}}{C_1} - \frac{x_2}{C_1} - \dot{x}_{1\text{ref}}\right) + kp(x_1 - x_{1\text{ref}}). \tag{12}$$

However, $e_1 = x_1 - x_{1\text{ref}}$.

Under this setting, Equation (12) is simplified as

$$\dot{V}_1 = e_1\left(\frac{i_{\text{PV}}}{C_1} - \frac{x_2}{C_1} - \dot{x}_{1\text{ref}} + kp\right). \tag{13}$$

We must ensure that $\dot{V}_1$ is negative definite. To this end, the first Lyapunov parameter, K_1, is introduced such that

$$\frac{i_{\text{PV}}}{C_1} - \frac{x_2}{C_1} - \dot{x}_{1\text{ref}} + kp = -K_1e_1, \quad K > 0. \tag{14}$$

Making x_2, subject in Equation (14) results to

$$x_2 = C_1\left(K_1e_1 + \frac{i_{\text{PV}}}{C_1} - \dot{x}_{1\text{ref}} + kp\right). \tag{15}$$

Consider Equation (15) as the reference virtual input. To this end, a deviation e_2 from the desired virtual input is introduced. Let φ be this reference. Therefore, Equation (15) is reformulated as follows:

$$\varphi = C_1\left(K_1e_1 + \frac{i_{\text{PV}}}{C_1} - \dot{x}_{1\text{ref}} + kp\right). \tag{16}$$

The error e_2 is now written as

$$e_2 = x_2 - \varphi. \tag{17}$$

Rearrange Equation (17) such that

$$x_2 = e_2 + \varphi. \tag{18}$$

Inserting Equation (18) into Equation (7) results to

$$\dot{e}_1 = \dot{x}_1 - \dot{x}_{1\text{ref}} = \frac{i_{\text{PV}}}{C_1} - \frac{e_2 + \varphi}{C_1} - \dot{x}_{1\text{ref}}. \tag{19}$$

Combining Equations (16) and (19) results to

$$\dot{e}_1 = \frac{i_{\text{PV}}}{C_1} - \frac{e_2 + C_1(K_1e_1 + (i_{\text{PV}}/C_1) - \dot{x}_{1\text{ref}} + kp)}{C_1} - \dot{x}_{1\text{ref}}. \tag{20}$$

Simplifying Equation (20), we have

$$\dot{e}_1 = -K_1e_1 - \frac{e_2}{C1} - kp. \tag{21}$$

Under this setting, Equation (11) becomes

$$\dot{V}_1 = e_1\dot{e}_1 + kp\dot{p} = e_1\left(-K_1e_1 - \frac{e_2}{C1} - kp\right) + kp\dot{p}. \tag{22}$$

Further simplifying Equation (22) with the fact that $p = \int_o^t e_1 dt$ and $\dot{p} = e_1$, we have that

$$\dot{V}_1 = -K_1e_1^2 - \frac{e_1e_2}{C_1}. \tag{23}$$

Since e_1 or e_2 can be either positive or negative, we have no idea of their state (sign) at any moment in the control loop, so we cannot conclude on the sign of e_1e_2/C_1. However, the first term $-K_1e_1^2$ will always be negative definite. Exploiting the derivatives of Equations (16) and (17), we have

$$\dot{e}_2 = \dot{x}_2 - \dot{\varphi}, \tag{24}$$

$$\dot{\varphi} = C_1\left(K_1\dot{e}_1 + \frac{\dddot{i}_{\mathrm{PV}}}{C_1} - \dddot{x}_{1\mathrm{ref}} + k\ddot{p}\right). \tag{25}$$

Simplifying Equation (25) using Equations (9) and (21), we have

$$\dot{\varphi} = C_1\left(K1\left(-K_1e_1 - \frac{e_2}{C1} - kp\right) + \frac{\dddot{i}_{\mathrm{PV}}}{C_1} - \dddot{x}_{1\mathrm{ref}} + k(x_1 - x_{1\mathrm{ref}}\right). \tag{26}$$

Inserting Equation (26) into (24) results to

$$\dot{e}_2 = \dot{x}_2 - C_1\left(K1\left(-K_1e_1 - \frac{e_2}{C1} - kp\right) + \frac{\dddot{i}_{\mathrm{PV}}}{C_1} - \dddot{x}_{1\mathrm{ref}} + k(x_1 - x_{1\mathrm{ref}})\right). \tag{27}$$

Further simplification of Equation (27) leads to

$$\dot{e}_2 = \dot{x}_2 - C_1\left(-K_1^2e_1 - \frac{K_1e_2}{C_1} - kK_1p + \frac{\dddot{i}_{\mathrm{PV}}}{C_1}\right) + C_1(\ddot{x}_{1\mathrm{ref}} - ke_1). \tag{28}$$

Under this setting, to guarantee the convergence of both errors to zero, a new Lyapunov function V_f is introduced. V_f is an augmented Lyapunov function. Its derivative must be negative. Therefore, let V_f be defined as follows

$$V_f = V_1 + \frac{1}{2}e_2^2. \tag{29}$$

Therefore, taking the time derivative of Equation (29), we have

$$\dot{V}_f = \dot{V}_1 + e_2\dot{e}_2. \tag{30}$$

Substituting Equation (23) in (30) results to

$$\dot{V}_f = -K_1e_1^2 - \frac{e_1e_2}{C_1} + e_2\dot{e}_2 = -K_1e_1^2 + e_2\left(\dot{e}_2 - \frac{e_1}{C_1}\right). \tag{31}$$

To ensure that Equation (31) is negative definite, we define

$$\dot{e}_2 - \frac{e_1}{C_1} = -K_2e_2. \tag{32}$$

Under this setting, Equation (21) combined with Equation (32) results to

$$\dot{V}_f = -K_1e_1^2 - K_2e_2^2. \tag{33}$$

Under this new setting, the Lyapunov law has been verified. The nonlinear control law is then deduced from Equations (4), (28), and (32).

$$-K_2e_2 = \frac{x_1}{L} - \frac{x_3}{L}(1-u) - C_1\left(-K_1^2e_1 - \frac{K_1e_2}{C_1} - kK_1p + \frac{\dddot{i}_{\mathrm{PV}}}{C_1}\right) + C_1(\ddot{x}_{1\mathrm{ref}} - ke_1) - \frac{e_1}{C_1}. \tag{34}$$

Further simplification of Equation (34) results to

$$u = 1 - \frac{L}{x_3}\left(K_2e_2 + \frac{x_1}{L} + K_1^2C_1e_1 + K_1e_2 + kK_1C_1p - \dddot{i}_{\mathrm{PV}} + C_1\dddot{x}_{1\mathrm{ref}} - C_1ke_1 - \frac{e_1}{C_1}\right). \tag{35}$$

The presence of derivative terms in the derived control law renders its practical implementation unfeasible due to the presence of noise during numerical differentiation. In this light, a higher-order sliding mode differentiator (HOSMD) designed in [49] is used to obtain in this situation a noiseless and robust nonlinear controller suitable for the boost converter control. The stability analysis and global convergence of the closed-loop system with the various subsystems, namely, the INC-IBSC and HOSMDs, are based on the separation principle theorem [49, 50] which permits the application of differentiation in nonlinear control. According to this principle, real-time robust exact differentiation is conceivable up to order L, provided that the next $(L+1)$th derivative is bounded by a known constant [51]. The finite-time convergence of the INC-IBSC and HOSMDs allows for the separate design of the control subblocks. Therefore, the separation principle is verified [51]. The main limitation of the practical implementation of this nonlinear controller is the satisfaction of the assumption on the boundedness of the state space variables in the operating domain. This assumption is fulfilled, given the convergence of INC-IBSC and HOSMDs and the nonlinear control law which warrants the global stability of the system.

6. Results and Discussions

Numerous investigations using numerical simulations, implemented in the MATLAB/Simulink environment, are performed to validate the performance of the proposed hybrid incremental conductance-integral backstepping controller under fast-changing operating conditions. The objective is to force the MSX-60-watt solar module [20] to operate at its maximum power point. Since most MPPT algorithms fail

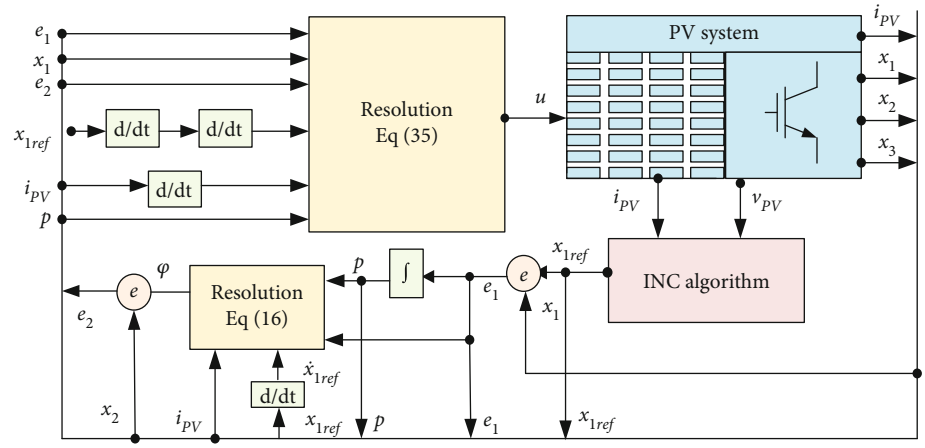

Figure 4: Numerical realization of the proposed hybrid INC-IBSC system.

under fast-changing operating conditions, we investigate the robustness of our systems under the most difficult operating scenarios involving fast-changing temperature, fast-changing irradiance, and abrupt variations in the load for robustness. The numerical realization of the proposed hybrid system is presented in Figure 4. At the simplest level, it shows that the incremental conductance algorithm (INC) is fed with measurements of the PV current and voltage. It outputs a reference voltage that is exploited by the nonlinear integral backstepping controller which is governed by Equations (16) and (35). The controller drives the PV system via a corresponding control law. The system is made up of a variable load and a boost converter with parameters input and output capacitor $C_1 = C_2 = 37\,\mu$F, inductor $L =$ 0.3 mH, and switching frequency of 250 kHz as shown on Table 1. The parameters of the controller as shown in Table 1, $[k, K_1, K_2]$, were obtained via the empirical method [43]. Resistances in the range of $15\,\Omega - 30\,\Omega$ are considered on the load side. The rest of this section is further subdivided as follows: in Subsection 6.1, the proposed hybrid INC-IBSC is evaluated at standard test conditions (STC). In Subsection 6.2, the results of the extended comparison with the classical incremental conductance (INC) algorithm are presented and discussed. The two systems are further evaluated and compared under changing load conditions at STC in Subsection 6.3. In Subsection 6.4, the systems are evaluated and compared under fast-changing irradiance and temperature scenarios in the presence of load variations. A comparison of the proposed hybrid INC-IBSC is provided in Subsection 6.5. Finally, validation of the proposed system with experimental data is provided in Subsection 6.6.

6.1. Evaluation of the Proposed Hybrid System at STC. The proposed hybrid system is first investigated at STC corresponding to the temperature of 25°C and irradiance of 1000 W/m^2. According to the characteristics of the considered PV module, a maximum power of 60 W and a maximum voltage of 16.70 V are expected under these conditions [21]. To this end, when the systems are subjected to the said conditions, the tracking of the MPP power and voltage is presented in Figures 5 and 6, respectively. The good MPP tracking potential of the proposed hybrid system can be appreciated in the power graph. A capture of the transient region reveals that the proposed hybrid system tracks the MPP at 0.77 ms. It is worth mentioning that the INC-IBSC controller exhibits overshoot as in Figure 6, the voltage tracking curve. This overshoot was measured at 11.51% from the reference MPP voltage. This explains the drop in power from 60 W to approximately 53.22 W during the transient as seen from the detailed view of the transient in Figure 5. It is worth appreciating that the controller rapidly restores the PV operating power and the voltage to the MPP in a time measured at $t_1 = 0.47$ ms, hence depicting the very good robustness of the controller. The overshoot occurrence is generally attributable to the integral action in the integral backstepping controller. The detailed transient view in Figure 5 tells the effect of the overshoot in a controller and its consequence on the power of the system. Though the integral action introduces some overshoot in the transient that is asymptotically decayed, the good steady-state response of the controller is preserved with the steady-state error of 0.12 V from the reference voltage. Hence, the efficiency of the controller was measured at 99.9434% according to the method described in [52].

Table 1: Parameters of the proposed system.

Parameters	Values
IBSC nonlinear controller $[k, K_1, K_2]$	[47.1853, 13750, 10000]
Boost converter $[L]$	0.3 mH
Boost $[C_1, C_2]$	[37 μF, 37 μF]
Load resistance $[R]$	[15 Ω, 25 Ω, 30 Ω]
Boost converter switching frequency $[F_s]$	250 kHz

6.2. Comparison of the Proposed Hybrid System with the INC at STC. In the vein of demonstrating the good performance of the proposed controller, it is compared with the conventional incremental conductance (INC) algorithm under the same operating conditions corresponding to STC. Their response to the said condition is presented in Figures 7

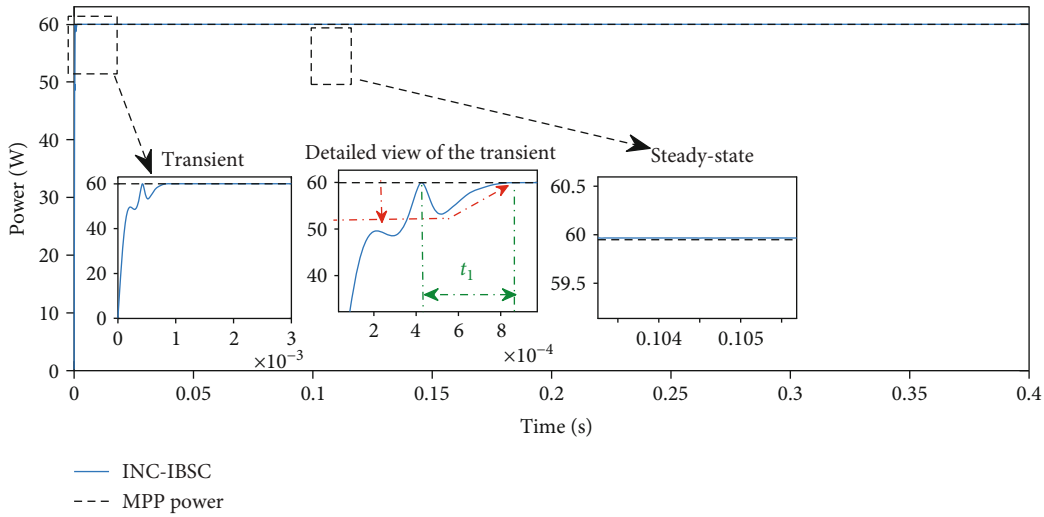

Figure 5: Tracking of the maximum power point (MPP) power with the hybrid INC-IBSC at STC.

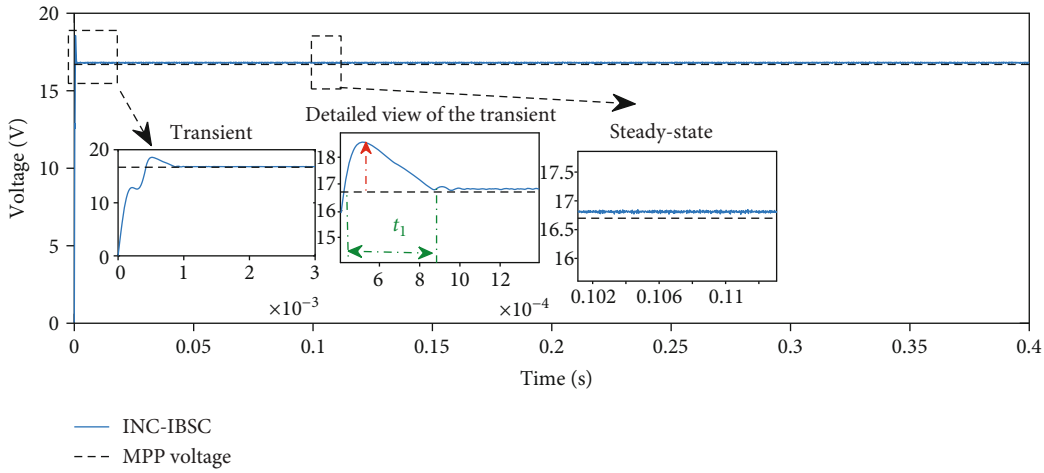

Figure 6: Tracking of the maximum power point (MPP) voltage with the hybrid INC-IBSC at STC.

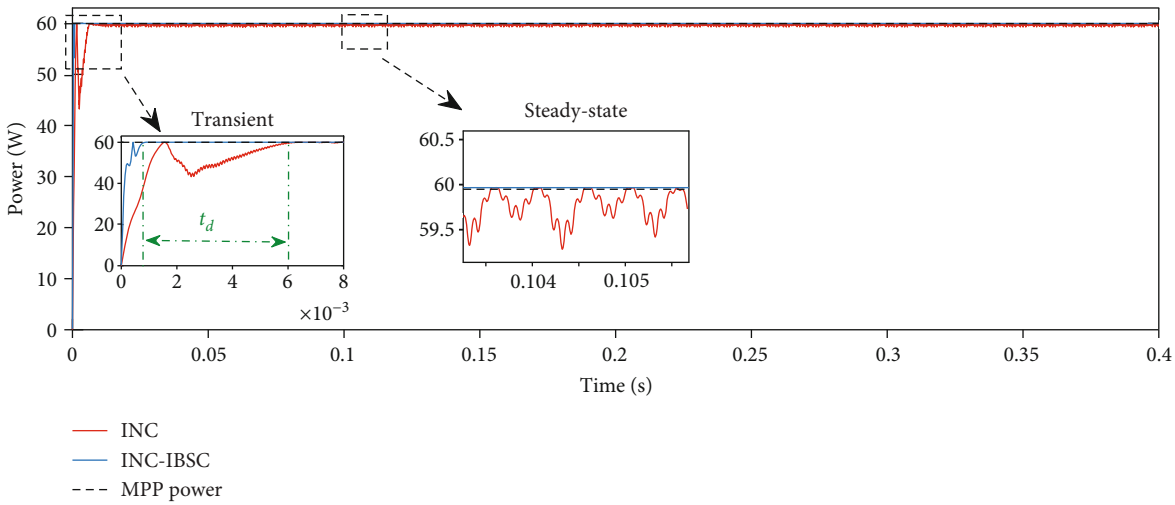

Figure 7: Tracking of the maximum power point (MPP) power with the INC and the hybrid INC-IBSC at STC.

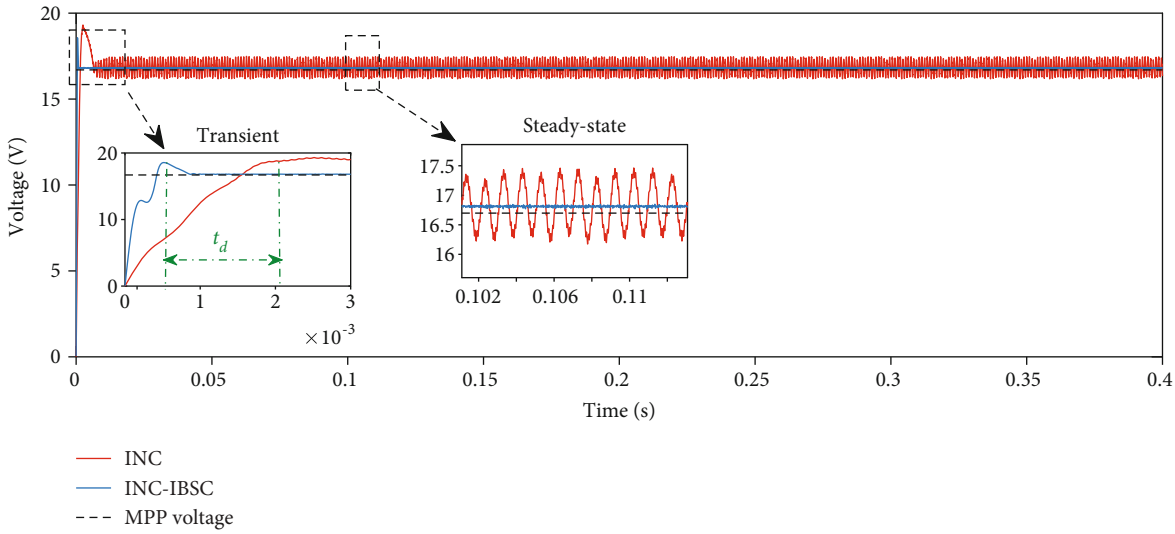

Figure 8: Tracking of the maximum power point (MPP) voltage with the INC and the hybrid INC-IBSC at STC.

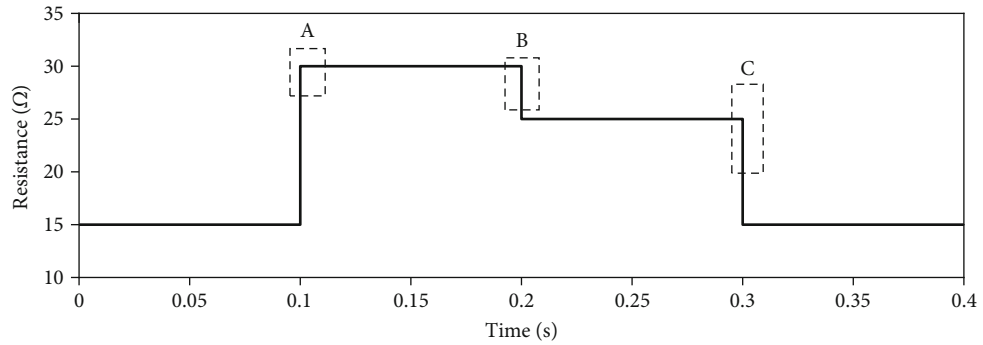

Figure 9: Load variation scenario.

and 8 for the tracking of the MPP power and voltage, respectively. It can be seen from these figures that the INC lags behind the proposed hybrid system in terms of tracking the MPP by a time t_d. Consequently, the INC tracked the MPP at 6.31 ms compared to the 0.77 ms of the hybrid system. Arithmetically, the proposed system is approximately 12 times faster than the INC MPPT. The relatively low steady-state performance of the INC can be confirmed in Figures 8. The INC continually oscillates at a steady state and will never gain stability. To this end, the efficiency of the INC was measured at 98.943 according to the method of [52]. Therefore, we conclude that the proposed hybrid system outperforms the conventional INC MPPT at STC.

6.3. Evaluation and Comparison of the Proposed Hybrid System with the INC at STC under Load Variation. The previous operating conditions are not sufficient to comment on the robustness of the proposed hybrid system. Therefore, to appreciate the robustness of the hybrid system, it is evaluated under abrupt variation in the load, and a comparison with the INC is also provided. Load variations are perceived in the system as disturbances because a change in load turns to alter the operating point of the PV. In this light, a robust MPPT controller must reject the effect of these changes by enforcing the operation at the MPP. To this end, the load variation scenarios considered in this investigation are presented in Figure 9.

The load variation scenario as depicted in Figure 9 involves three instances of abrupt load variations, labeled on the figure as A, B, and C at the time instant 0.1 s, 0.2 s, and 0.3 s, respectively. The systems are subjected to a constant load of value 15 Ω, up to the time instant at A (0.1 s) when the load instantaneously steps up to30 Ω. From this instant, it is held constant up to 0.2 s (B), when the load abruptly steps down to25 Ω, and kept constant up to 0.3 s (C). At 0.3 s, the load is restored to its initial value of 15 Ω and held constant till 0.4 s. Under this sequence of load variations, the power and voltage tracked by the INC and the proposed hybrid INC-IBSC are presented in Figures 10 and 11, respectively. At the different instances of load variation, it can be seen that the INC-IBSC ensures the stability of the PV operating point at the MPP. From a detailed evaluation point of view, it is measured that when the load changes from 15 Ω to 30 Ω at 0.1 s, the power under the control of the INC drops by 14.03 W, and the voltage increases by 2.38 V, the operating point is only restored after 4.20 ms of

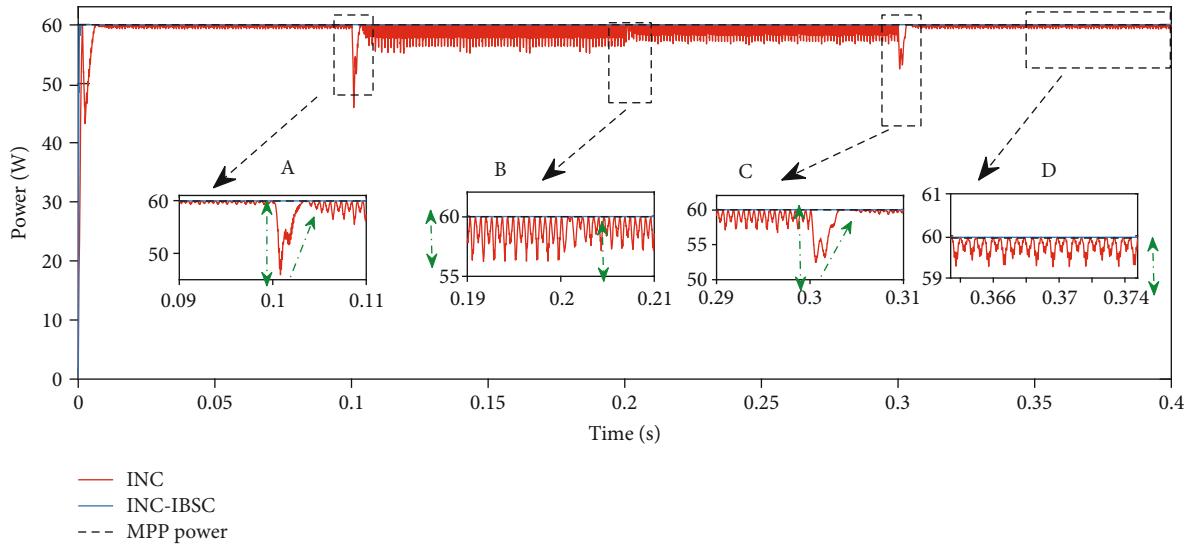

Figure 10: Tracking of the maximum power point (MPP) power with the INC and the hybrid INC-IBSC at STC under load variation scenarios.

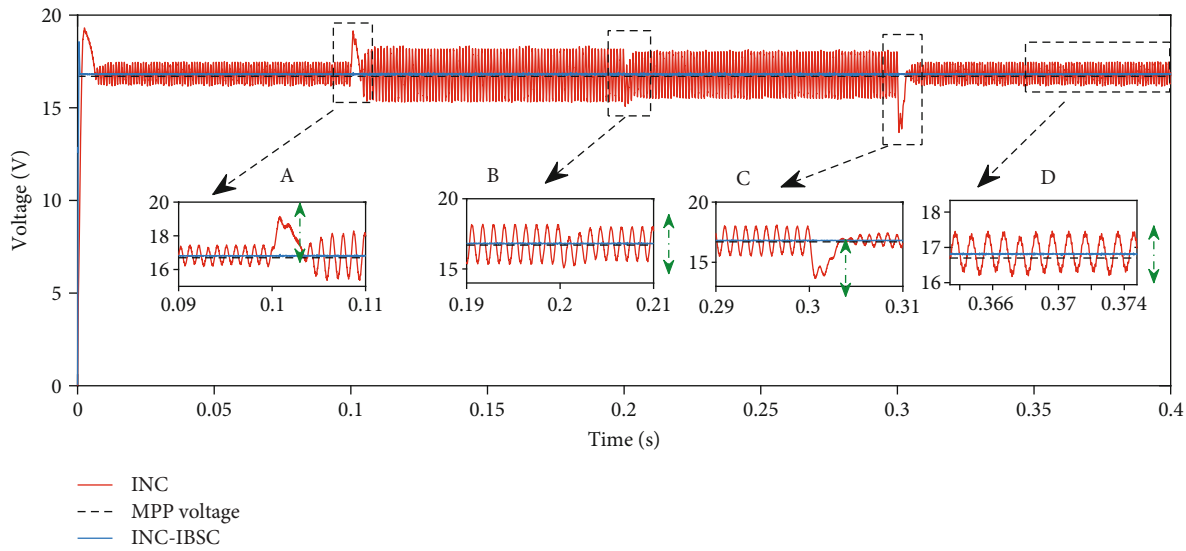

Figure 11: Tracking of the maximum power point (MPP) voltage with the INC and the hybrid INC-IBSC at STC under load variation scenarios.

time elapsed, after which the power and voltage continue to oscillate. At this same instant, the voltage and power of the PV under the control of the proposed hybrid INC-IBSC stay at the MPP, as presented in the generalization in Table 2. At B, when the load value drops from 30 Ω to 25 Ω, it is measured that the PV power drops from the MPP by approximately 2.95 W after which it is restored in 1.8 ms and continues to oscillate. At this same instant, the proposed hybrid system ensures that the PV system operates at MP. The complete comparison of the two systems at the instants A, B, and C is presented in Table 3. Generally, one can note that the proposed system has very good robustness against load disturbances. More to that, it delivers an efficiency of 98.9449% under the aforementioned load variation scenario.

Table 2: Characteristics of the MSX-60W [23].

PV parameters	Value
Maximum power (P_{mpp})	60 W
Voltage at maximum power (V_{mpp})	16.7 V
Current at maximum power (I_{mpp})	3.59 A
Open circuit voltage (V_{oc})	21.1
Short-circuit current (I_{sc})	3.8 A
Temperature coefficient of V_{oc}	-80 mV/°C
Temperature coefficient of I_{sc}	-0.065%/°C

Table 3: Evaluation and comparison of the proposed INC-IBSC with the INC under changing load at STC.

MPPT system	$\downarrow P_{pv} \cap \uparrow t_s$ A (W $\cap$ ms)	$\downarrow P_{pv} \cap \uparrow t_s$ B (W $\cap$ ms)	$\downarrow P_{pv} \cap \uparrow t_s$ C (W $\cap$ ms)	$\Delta V_{pv} \cap \uparrow t_s$ A(V $\cap$ *ms*)	$\Delta V_{pv} \cap \uparrow t_s$ B (V $\cap$ ms)	$\Delta V_{pv} \cap \uparrow t_s$ C (V $\cap$ ms)	Efficiency (%)
INC	14.03 $\cap$ 4.20	2.95 $\cap$ ~ 1.8	6.81 $\cap$ 3.7	2.38 $\cap$ 4.20	1.58 $\cap$ 0.5	2.8 $\cap$ 3.6	98.5124
INC-IBSC	0 $\cap$ 0	0 $\cap$ 0	0 $\cap$ 0	0 $\cap$ 0	0 $\cap$ 0	0 $\cap$ 0	99.9449

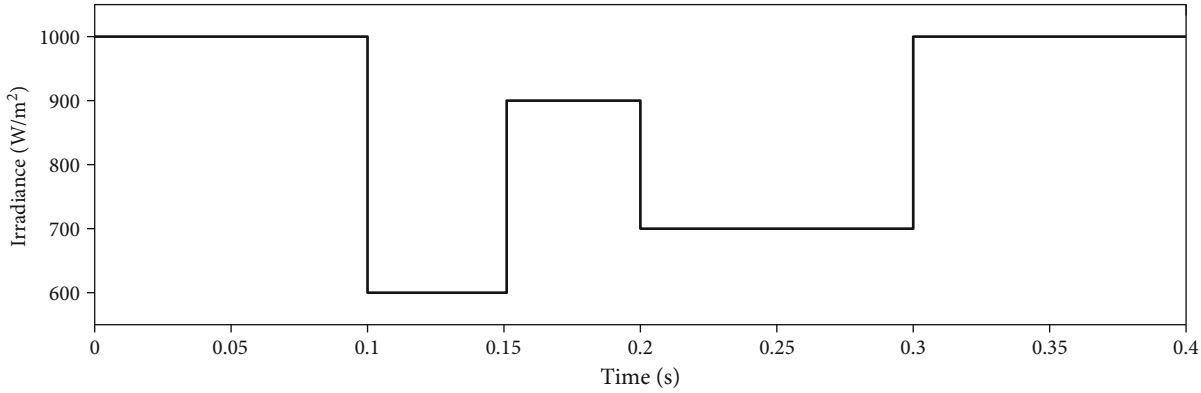

Figure 12: Fast-changing operating irradiance scenario.

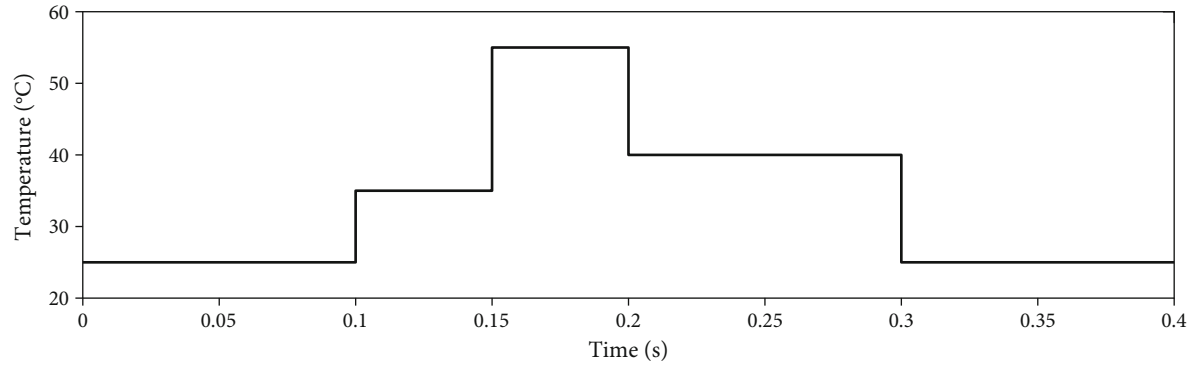

Figure 13: Fast-changing operating temperature scenario.

In Table 3, the notations $\downarrow P_{pv} \cap t_s$ and $\downarrow P_{pv}$ represent the drop in power from the MPP at the instant of the load variation (A, B, or C) and t_s is the time taken to restore the operating point to the MPP. In the notation, W $\cap$ ms, W (watts) is the unit of power, and ms (millisecond) is the unit of time. In the notation $\Delta V_{pv} \cap t_s$, ΔV_{pv} is the deviation of the voltage operating point from the MPP voltage.

6.4. Evaluation and Comparison of the Proposed Hybrid System with the INC under Fast-Changing Environmental Conditions and Load Variation Scenarios. The proposed hybrid INC-IBSC system and the INC are now subjected to the worst operating conditions. The objective of this test is to evaluate and appreciate the feasibility of the proposed MPPT system and its better robustness against difficult operating scenarios. In this vein, both systems are subjected to the same load variation profile as was described in Figure 9 and to fast-changing irradiance and temperature as depicted in Figures 12 and 13, respectively. It can be seen in Figures 14 and 15 for the voltage and power tracking that the proposed system has a far better dynamic performance than the INC, as it maintains the good stability of the operating point at the MPP.

6.5. Comparison of the Proposed Hybrid INC-IBSC with Other Controllers and Techniques from the Literature. The proposed MPPT system operates the PV at 99.9434% efficiency under standard test conditions with steady-state ripples measured at 0.294% peak to peak in volts. When compared with 8 recently published MPPT algorithm (controller) methods from the literature, it is appreciated that the proposed MPPT system presents a superior performance. The table of performance comparisons at standard test conditions is presented in Table 4.

6.6. Real-Time Validation with Experimental Data. In practice, a PV system is subjected to continually changing

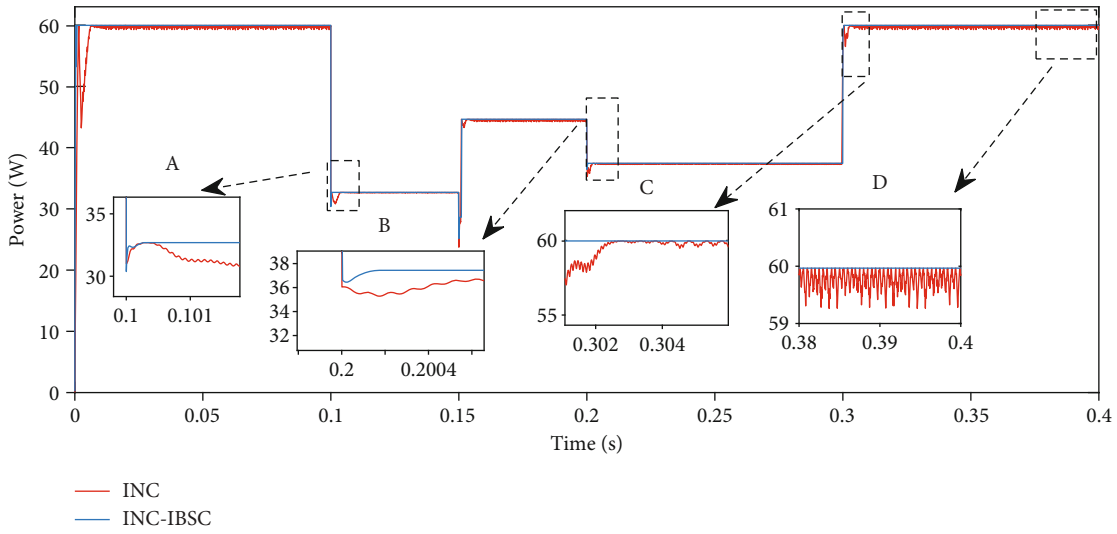

Figure 14: Tracking of the maximum power point (MPP) power with the INC and the hybrid INC-IBSC under load variation scenarios and fast-changing environmental conditions.

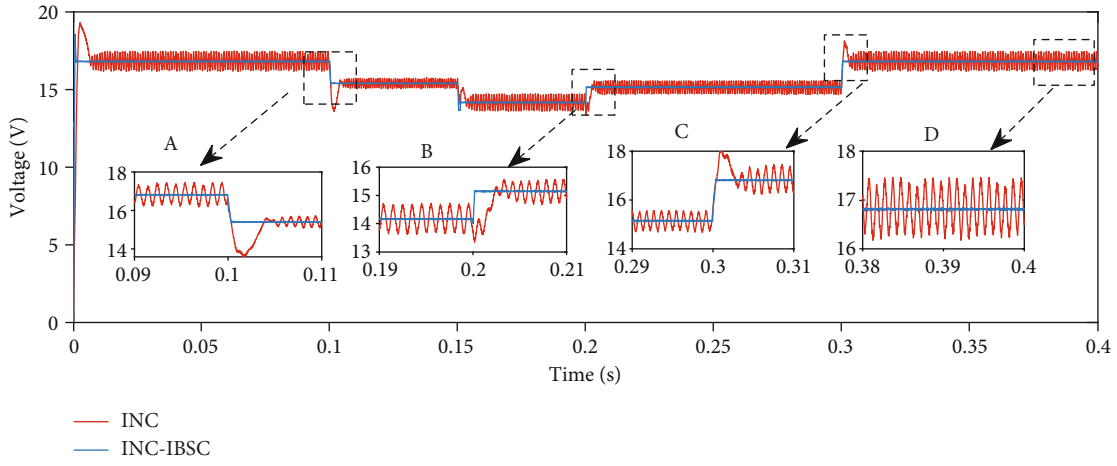

Figure 15: Tracking of the maximum power point (MPP) voltage with the INC and the hybrid INC-IBSC at under load variation scenarios and fast-changing environmental conditions.

Table 4: Comparison of the proposed MPPT with other MPPT methods in the literature under STC.

Ref	Year	DC-DC converter type	MPPT algorithm (controller)	Tracking time (ms)	Ripples (peak to peak)	Efficiency (%)
[53]	2021	Boost	Novel MPPT tactic	9.6	x	99.86
[54]	2022	Boost	Innovative MPPT	10	x	99.75
[55]	2021	Boost	Thermal imaging-based P&O	220	x	x
[56]	2020	Boost	Extremum seeking	2500	x	X
[57]	2022	Boost	Advanced MPPT	11	x	99.8
[43]	2018	Buck	Backstepping	1.5	0.9	x
[45]	2018	Non-Inverting Buck boost	Integral backstepping Controller	2.2	0.63	x
[58]	2021	Boost	Backstepping-sliding mode controller	10	x	x
Proposed	—	Boost	Proposed	0.4	0.17%	99.9434%

x in the table signifies that the respective parameter was not defined by the author.

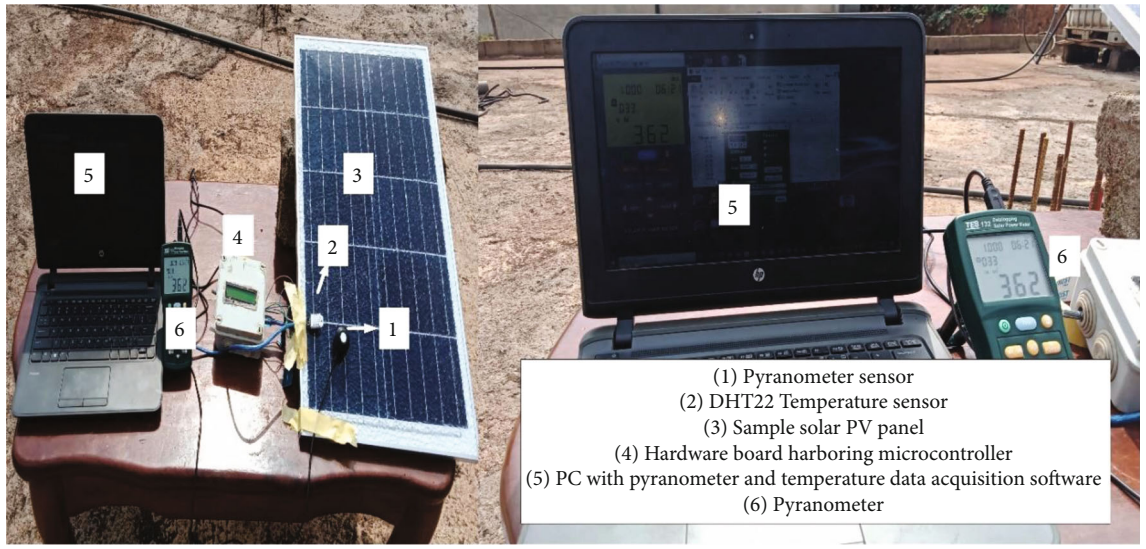

Figure 16: Experimental set-up for recording real-time solar irradiance and temperature on the PV.

Table 5: Experimental data of solar irradiance and temperature.

No.	Irr (W/m^2)	T (°C)	No.	Irr (W/m^2)	T (°C)	No.	Irr (W/m^2)	T (°C)	No.	Irr (W/m^2)	T (°C)
1	270	31.8	10	520	46.1	19	1008	55.9	28	785	33.5
2	340	33.5	11	437	38.4	20	1025	47.5	29	501	31.6
3	345	35	12	1162	42.9	21	650	39.5	30	405	33
4	305	34.8	13	886	40.5	22	447	37.8	31	423	31.4
5	400	37.8	14	505	43.8	23	401	39	32	340	29
6	259	36	15	1091	45	24	500	34.9	33	339	28.6
7	451	45.2	16	1120	44.6	25	626	34.5			
8	362	40.6	17	1044	53.1	26	740	34.7			
9	419	39.3	18	1095	55.4	27	525	33			

environmental conditions. Hence, to validate the proposed MPPT controller, it was subjected to real-time experimental data. The experimental set-up as presented in Figure 16 was made of a pyranometer for irradiance measurement, the DHT22 temperature sensor, a sample solar PV panel, an Arduino mega microcontroller, and a computer equipped with data logging applications. The experimental set-up was mounted in the city of Dschang, West Province of Cameroon, on January 5, 2022. Data corresponding to the PV irradiance and temperature were collected and resampled at 15 minutes, corresponding to 8:30 am to 4:30 pm, and represented by 33 data points as shown in Table 5.

The 33 data points as shown in Table 5 were scaled to 40000 data points for a running time of 0.4 seconds in MATLAB/Simulink environment. The maximum experimental irradiance of 1162 W/m^2 occurred at noon (Table 5) corresponding to 0.138 seconds on the scaled signal as inferred from Figure 17. On the other hand, the minimum irradiance of 270 W/m^2 occurs at the very first sample instant, both for Table 5 and Figure 17. Moreover, it can be seen that the temperature was, respectively, maximum (55.9°C) and minimum (28.6°C) at 1:00 pm and 4:40 pm, inferred from Table 5, and at the 0.225 s and 0.4 s instant, inferred from Figure 17.

The proposed hybrid INC-IBSC, with its realization in Figure 4, was subjected to the experimental conditions of Figure 17 in a MATLAB/Simulink environment. Therefore, the validation involves assessing the proposed MPPT system in response to the experimental environmental conditions of Figure 17. To comment on the performance of the proposed system in the aforementioned condition, a corresponding comparison was attained with the INC.

In response to experimental environmental conditions, the power response of both the proposed INC-IBSC and INC is presented in Figure 18. Viewing from the tracking line in Figure 18, image (i), it can be seen that the proposed INC-IBSC tracks the maximum power at 1.7 ms while the INC tracks at 6.9 ms. This conveys that the INC-IBSC is approximately 4 times faster than the INC under experimental conditions. Furthermore, we note that these tracking times are in good agreement with the 6.3 ms and 0.77 ms obtained at STC in nonexperimental environmental conditions, which is in Figure 7 and discussed in Subsection 6.2. However, the respective tracking times increased by 0.6 ms for the INC and by 0.93 ms for the proposed INC-IBSC. This increase is attributable to the fact that conditions are more dynamic under the experimental conditions than those at

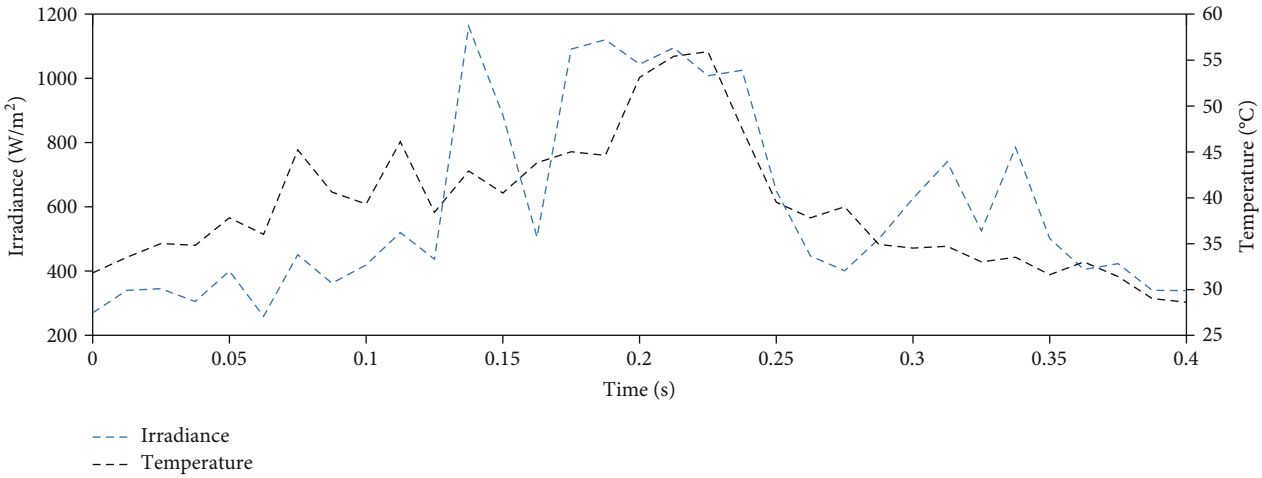

Figure 17: Experimental irradiance and temperature for 8:30 am to 4:30 pm, scaled up to 0.4 seconds.

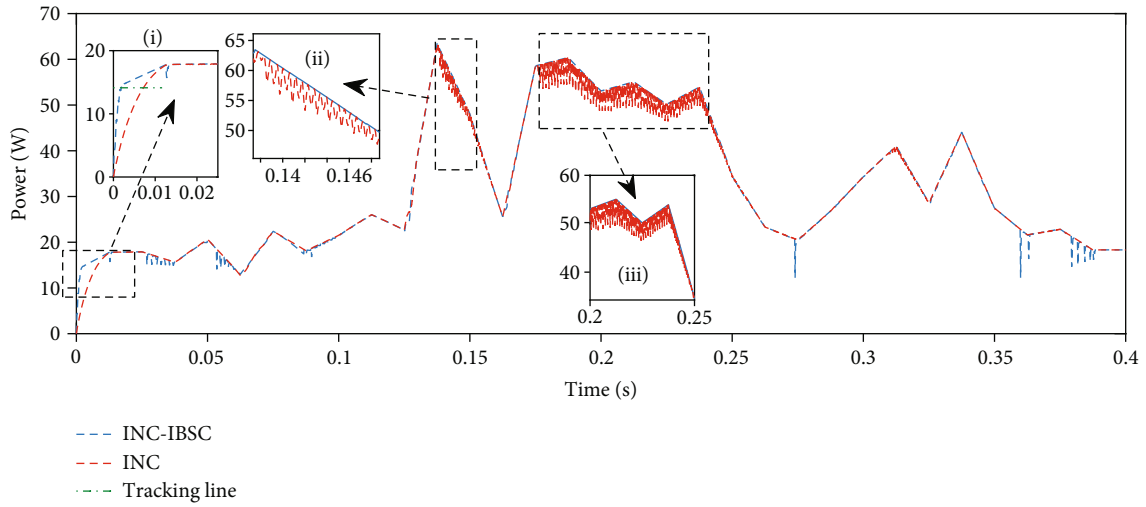

Figure 18: Power response of the proposed INC-IBSC and INC to the experimental conditions.

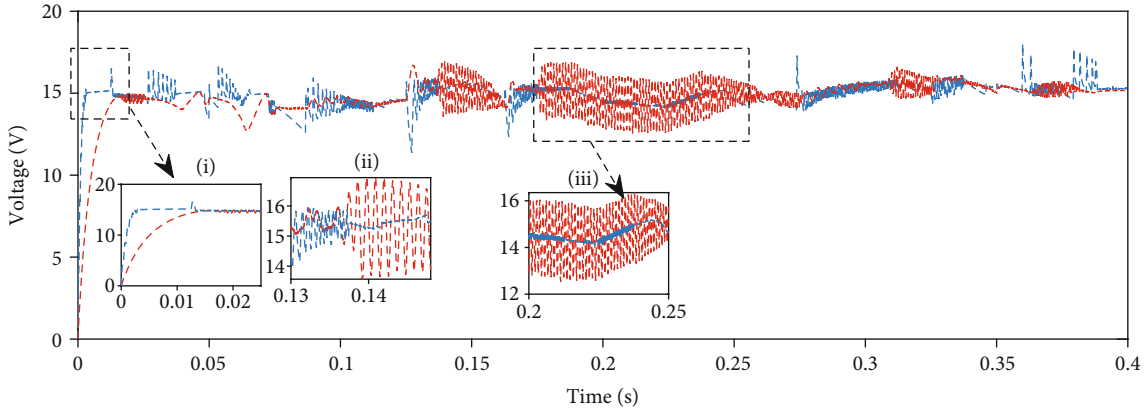

Figure 19: Voltage response of the proposed INC-IBSC and INC to the experimental conditions.

STC. It is therefore confirmed that the proposed INC-IBSC is faster than the INC.

Moreover, it is worth exalting the better dynamic response of the proposed INC-IBSC, relative to INC. Inferences from Figure 18, internal images (i) and (ii), show that the INC exhibits consistent power oscillation, a situation which is palliated by the INC-IBSC. Numerically integrating the area under both power curves using the trapezoidal method, it is found that the INC yields 12.51 W/s while the proposed system yields 12.70 W/s of energy. This is a confirmation that from an energy extraction point of view, the proposed INC-IBSC is better than the INC. The lower energy yield of the INC amounts to its slow tracking speed and relatively poor dynamic response.

From a voltage response point of view and with inference from Figure 19, it is further confirmed that the proposed INC-IBSC has a better dynamic response than the INC. This is obvious given the nonlinear and robust capacities of the INC-IBSC. The faster tracking performance of the proposed INC-IBSC relative to the INC is reconfirmed from internal image (i). The internal image (ii) reveals that the proposed system indeed exhibits voltage oscillations, however lower than the INC, a scenario that is confirmable from internal image (iii) on the same figure.

7. Conclusion

A hybrid incremental conductance-integral backstepping nonlinear controller was proposed for efficient control and effective maximum energy harvesting from a PV system under fast-changing operating conditions. The proposed hybrid system exploits the benefits of the incremental conductance (INC) algorithm in searching for the maximum power point (MPP) to generate a reference voltage that feeds a Lyapunov-based integral backstepping controller. The hybrid MPPT controller demonstrated exceptional performances and palliated the performance limitations of the isolated INC MPPT algorithm. By evaluation and comparisons, it was found better than the INC and 8 other recently published MPPT methods from the literature. An extended validation under experimental environmental conditions showed that the hybrid system is approximately four times faster than the INC in tracking the maximum power with better energy yield than the latter. The above work has been applied to a PV system under uniform irradiance conditions. It is suggested that future works be directed towards the extension of the proposed hybrid MPPT controller to PV systems under the effects of partial shading.

A new hybrid incremental conductance-integral backstepping nonlinear MPPT controller was proposed in this paper.

Data Availability

All the data used to support the findings of this study are included within the paper.

Conflicts of Interest

The authors declare that they have no conflicts of interest.

References

[1] ""Energy and climate," *Federal Ministry for Economic Cooperation and Development*," 2022, https://www.bmz.de/en/issues/climate-change-and-development/energy-and-climate.

[2] United Nations, *The Paris Agreement*, United Nations, 2021, https://www.un.org/en/climatechange/paris-agreement.

[3] P. A. Owusu and S. Asumadu-Sarkodie, "A review of renewable energy sources, sustainability issues and climate change mitigation," *Cogent Engineering*, vol. 3, no. 1, 2016.

[4] M. Z. Jacobson, M. A. Delucchi, M. A. Cameron, and B. V. Mathiesen, "Matching demand with supply at low cost in 139 countries among 20 world regions with 100% intermittent wind, water, and sunlight (WWS) for all purposes," *Renewable Energy*, vol. 123, pp. 236–248, 2018.

[5] A. Sadiqa, A. Gulagi, and C. Breyer, "Energy transition roadmap towards 100% renewable energy and role of storage technologies for Pakistan by 2050," *Energy*, vol. 147, pp. 518–533, 2018.

[6] M. J. B. Kabeyi and O. A. Olanrewaju, "Sustainable energy transition for renewable and low carbon grid electricity generation and supply," *Frontiers in Energy Research*, vol. 9, 2022.

[7] F. Dinçer, "The analysis on photovoltaic electricity generation status, potential and policies of the leading countries in solar energy," *Renewable and Sustainable Energy Reviews*, vol. 15, no. 1, pp. 713–720, 2011.

[8] A. Harrison, J. D. D. N. Ndongmo, N. H. Alombah et al., "Robust Nonlinear control of Maximum Power Point Tracking in PV solar energy system under real environmental conditions," *ASEC*, vol. 31, no. 1, 2022.

[9] A. Shahdadi, S. M. Barakati, and A. Khajeh, "Design and implementation of an improved sliding mode controller for maximum power point tracking in a SEPIC based on PV system," *Engineering Reports*, vol. 1, no. 4, 2019.

[10] J. Ahmed and Z. Salam, "A critical evaluation on maximum power point tracking methods for partial shading in PV systems," *Renewable and Sustainable Energy Reviews*, vol. 47, pp. 933–953, 2015.

[11] B. K. Bose, P. M. Szczesny, and R. L. Steigerwald, "Microcomputer control of a residential photovoltaic power conditioning system," *IEEE Transactions on Industry Applications*, vol. IA-21, no. 5, pp. 1182–1191, 1985.

[12] T. Esram and P. L. Chapman, "Comparison of photovoltaic array maximum power point tracking techniques," *IEEE Transactions on Energy Conversion*, vol. 22, no. 2, pp. 439–449, 2007.

[13] N. Femia, G. Petrone, G. Spagnuolo, and M. Vitelli, "Optimization of perturb and observe maximum power point tracking method," *IEEE Transactions on Power Electronics*, vol. 20, no. 4, pp. 963–973, 2005.

[14] G. J. Kish, J. J. Lee, and P. W. Lehn, "Modelling and control of photovoltaic panels utilising the incremental conductance method for maximum power point tracking," *IET Renewable Power Generation*, vol. 6, no. 4, p. 259, 2012.

[15] A. Safari and S. Mekhilef, "Simulation and hardware implementation of incremental conductance MPPT with direct

control method using Cuk converter," *IEEE Transactions on Industrial Electronics*, vol. 58, no. 4, pp. 1154–1161, 2011.

[16] A. Reza Reisi, M. Hassan Moradi, and S. Jamasb, "Classification and comparison of maximum power point tracking techniques for photovoltaic system: a review," *Renewable and Sustainable Energy Reviews*, vol. 19, pp. 433–443, 2013.

[17] M. A. Eltawil and Z. Zhao, "MPPT techniques for photovoltaic applications," *Renewable and Sustainable Energy Reviews*, vol. 25, pp. 793–813, 2013.

[18] J. Ramos-Hernanz, I. Uriarte, J. M. Lopez-Guede, U. Fernandez-Gamiz, A. Mesanza, and E. Zulueta, "Temperature based maximum power point tracking for photovoltaic modules," *Scientific Reports*, vol. 10, no. 1, p. 12476, 2020.

[19] B. Subudhi and R. Pradhan, "A comparative study on maximum power point tracking techniques for photovoltaic power systems," *IEEE Transactions on Sustainable Energy*, vol. 4, no. 1, pp. 89–98, 2013.

[20] A. Harrison, E. M. Nfah, J. de Dieu Nguimfack Ndongmo, and N. H. Alombah, "An enhanced P&O MPPT algorithm for PV systems with fast dynamic and steady-state response under real irradiance and temperature conditions," *International Journal of Photoenergy*, vol. 2022, Article ID 6009632, 21 pages, 2022.

[21] N. Kumar, B. Singh, and B. K. Panigrahi, "Voltage sensorless based model predictive control with battery management system: for solar PV powered on-board EV charging," *IEEE Transactions on Transportation Electrification*, pp. 1–1, 2022.

[22] P. Kumari, N. Kumar, and B. K. Panigrahi, "A framework of reduced sensor rooftop SPV system using parabolic curve fitting MPPT technology for household consumers," *IEEE Transactions on Consumer Electronics*, vol. 69, no. 1, pp. 29–37, 2023.

[23] I. V. Banu, R. Beniugă, and M. Istrate, "Comparative analysis of the perturb-and-observe and incremental conductance MPPT methods," in *2013 8Th International Symposium on advanced topics in electrical engineering (ATEE)*, pp. 1–4, Bucharest, Romania, 2013, https://ieeexplore.ieee.org/abstract/document/6563483.

[24] A. Al-Diab and C. Sourkounis, "Variable step size P&O MPPT algorithm for PV systems," in *2010 12th international conference on optimization of electrical and electronic equipment*, pp. 1097–1102, Brasov, Romania, 2010, http://ieeexplore.ieee.org/document/5510441/.

[25] M. H. Osman and A. Refaat, "Adaptive multi-variable step size P&O MPPT for high tracking-speed and accuracy," in *IOP Conference Series: Materials Science and Engineering*, vol. 643, 2019, no. 1, Article ID 012050.

[26] S. Jain and V. Agarwal, "A new algorithm for rapid tracking of approximate maximum power point in photovoltaic systems," *IEEE Power Electronics Letters*, vol. 2, no. 1, pp. 16–19, 2004.

[27] X. Li, H. Wen, L. Jiang, E. G. Lim, Y. Du, and C. Zhao, "Photovoltaic modified β-parameter-based MPPT method with fast tracking," *Journal of Power Electronics*, vol. 16, no. 1, pp. 9–17, 2016.

[28] X. Li, H. Wen, and C. Zhao, "Improved beta parameter based MPPT method in photovoltaic system," in *2015 9th International Conference on Power Electronics and ECCE Asia (ICPE-ECCE Asia)*, pp. 1405–1412, Seoul, Korea (South), 2015, https://ieeexplore.ieee.org/document/7167963?arnumber=7167963.

[29] H. Elaissaoui, M. Zerouali, A. E. Ougli, and B. Tidhaf, "MPPT algorithm based on fuzzy logic and artificial neural network (ANN) for a hybrid solar/wind power generation system," in *2020 Fourth international conference on intelligent computing in data sciences (ICDS)*, pp. 1–6, Fez, Morocco, 2020.

[30] A. Al Nabulsi and R. Dhaouadi, "Efficiency optimization of a DSP-based standalone PV system using fuzzy logic and dual-MPPT control," *IEEE Transactions on Industrial Informatics*, vol. 8, no. 3, pp. 573–584, 2012.

[31] A. El Khateb, N. A. Rahim, J. Selvaraj, and M. N. Uddin, "Fuzzy-logic-controller-based SEPIC converter for maximum power point tracking," *IEEE Transactions on Industry Applications*, vol. 50, no. 4, pp. 2349–2358, 2014.

[32] M. A. A. M. Zainuri, N. A. Rahim, A. Che Soh, and M. A. M. Radzi, "Development of adaptive perturb and observe-fuzzy control maximum power point tracking for photovoltaic boost dc–dc converter," *IET Renewable Power Generation*, vol. 8, no. 2, pp. 183–194, 2014.

[33] G. Calvinho, J. Pombo, S. Mariano, and M. do Rosario Calado, "Design and implementation of MPPT system based on PSO algorithm," in *2018 International conference on intelligent systems (IS)*, pp. 733–738, Funchal, Portugal, 2018.

[34] S. Titri, C. Larbes, K. Y. Toumi, and K. Benatchba, "A new MPPT controller based on the ant colony optimization algorithm for photovoltaic systems under partial shading conditions," *Applied Soft Computing*, vol. 58, pp. 465–479, 2017.

[35] B. Laxman, A. Annamraju, and N. V. Srikanth, "A grey wolf optimized fuzzy logic based MPPT for shaded solar photovoltaic systems in microgrids," *International Journal of Hydrogen Energy*, vol. 46, no. 18, pp. 10653–10665, 2021.

[36] S. Mohanty, B. Subudhi, and P. K. Ray, "A new MPPT design using grey wolf optimization technique for photovoltaic system under partial shading conditions," *IEEE Transactions on Sustainable Energy*, vol. 7, no. 1, pp. 181–188, 2016.

[37] N. Vázquez, Y. Azaf, I. Cervantes, E. Vázquez, and C. Hernández, "Maximum power point tracking based on sliding mode control," *International Journal of Photoenergy*, vol. 2015, Article ID e380684, 8 pages, 2015.

[38] S. Marripudi, S. K. Gudey, and G. R. Gujju, "Analysis and design of sliding mode control for MPPT based PV system with a battery storage," in *2017 14th IEEE India Council International Conference (INDICON)*, pp. 1–6, Roorkee, India, 2017, https://ieeexplore.ieee.org/document/8487481.

[39] A. Hameed, H. S. Zad, A. Ulasyar, and J. Hashim, "Robust sliding mode control based maximum power point tracking of solar photovoltaic system," in *2020 3rd International Conference on Computing, Mathematics and Engineering Technologies (iCoMET)*, pp. 1–6, Sukkur, Pakistan, 2020, https://ieeexplore.ieee.org/document/9073886.

[40] R. Ayat, A. Bouafia, and J. Gaubert, "Experimental validation of synergetic approach based MPPT controller for an autonomous PV system," *IET Renewable Power Generation*, vol. 15, no. 7, pp. 1515–1527, 2021.

[41] D. Zehar, A. Chérif, K. Benmahammed, and K. Behih, "Fast terminal synergetic control of underactuated system," in *2018 15th International Multi-Conference on Systems, Signals & Devices (SSD)*, pp. 1184–1189, Yasmine Hammamet, Tunisia, 2018, https://www.semanticscholar.org/paper/Fast-Terminal-Synergetic-Control-of-Underactuated-Zehar-Ch%C3%A9rif/9376a5af5b7d6b384f7ffd265aff8ce04cae6345.

[42] N. Mars, F. Grouz, N. Essounbouli, and L. Sbita, "Synergetic MPPT controller for photovoltaic system," *Journal of Electrical & Electronic Systems*, vol. 6, no. 2, p. 2332, 2017.

[43] R. Iftikhar, I. Ahmad, M. Arsalan, N. Naz, N. Ali, and H. Armghan, "MPPT for photovoltaic system using nonlinear controller," *International Journal of Photoenergy*, vol. 2018, Article ID 6979723, 11 pages, 2018.

[44] R. S. Butt, I. Ahmad, R. Iftikhar, and M. Arsalan, "Integral backstepping and synergetic control for tracking of infected cells during early antiretroviral therapy," *IEEE Access*, vol. 7, pp. 69447–69455, 2019.

[45] M. Arsalan, R. Iftikhar, I. Ahmad, A. Hasan, K. Sabahat, and A. Javeria, "MPPT for photovoltaic system using nonlinear backstepping controller with integral action," *Solar Energy*, vol. 170, pp. 192–200, 2018.

[46] K. Ali, Q. Khan, S. Ullah, I. Khan, and L. Khan, "Nonlinear robust integral backstepping based MPPT control for standalone photovoltaic system," *PLoS One*, vol. 15, no. 5, article e0231749, 2020.

[47] M. A. Elgendy, B. Zahawi, and D. J. Atkinson, "Assessment of the incremental conductance maximum power point tracking algorithm," *IEEE Transactions on Sustainable Energy*, vol. 4, no. 1, pp. 108–117, 2013.

[48] R. D. Middlebrook and S. Ćuk, "A general unified approach to modelling switching-converter power stages," *International Journal of Electronics*, vol. 42, no. 6, pp. 521–550, 1977.

[49] G. Kenne, J. D. Ndongmo, R. F. Kuate, and H. B. Fotsin, "An online simplified nonlinear controller for transient stabilization enhancement of DFIG in multi-machine power systems," *IEEE Transactions on Automatic Control*, vol. 60, no. 9, pp. 2464–2469, 2015.

[50] J. de Dieu Nguimfack-Ndongmo, G. Kenné, and E. M. Nfah, "Design of nonlinear synergetic controller for transient stabilization enhancement of DFIG in multimachine wind power systems," *Energy Procedia*, vol. 93, pp. 125–132, 2016.

[51] A. Levant, "Higher-order sliding modes, differentiation and output-feedback control," *International Journal of Control*, vol. 76, no. 9–10, pp. 924–941, 2003.

[52] N. Femia, *Power Electronics and Control Techniques for Maximum Energy Harvesting in Photovoltaic Systems*, Crc Press, Taylor & Francis Group, Boca Raton, 2013.

[53] A. Chellakhi, S. El Beid, and Y. Abouelmahjoub, "Implementation of a novel MPPT tactic for PV system applications on MATLAB/Simulink and Proteus-based Arduino board environments," *International Journal of Photoenergy*, vol. 2021, Article ID 6657627, 19 pages, 2021.

[54] A. Chellakhi, S. El Beid, and Y. Abouelmahjoub, "An innovative fast-converging speed MPPT approach without oscillation for temperature varying in photovoltaic systems applications," *Energy Sources, Part A: Recovery, Utilization, and Environmental Effects*, vol. 44, no. 2, pp. 2674–2696, 2022.

[55] I. Khan and S. Khan, "Thermal imaging based maximum power point tracking for solar modules in variable ambient temperature," *SN Applied Sciences*, vol. 3, no. 5, p. 536, 2021.

[56] A. F. Tchouani Njomo, G. Kenne, R. M. Douanla, and L. L. Sonfack, "A modified ESC algorithm for MPPT applied to a photovoltaic system under varying environmental conditions," *International Journal of Photoenergy*, vol. 2020, Article ID 1956410, 15 pages, 2020.

[57] A. Chellakhi, S. El Beid, and Y. Abouelmahjoub, "An advanced MPPT scheme for PV systems application with less output ripple magnitude of the boost converter," *International Journal of Photoenergy*, vol. 2022, Article ID 2133294, 21 pages, 2022.

[58] K. Behih and H. Attoui, "Backstepping terminal sliding mode MPPT controller for photovoltaic systems," *Engineering, Technology & Applied Science Research*, vol. 11, no. 2, pp. 7060–7067, 2021.